Solar Energy Materials & Solar Cells 132 (2015) 443–449

Contents lists available at ScienceDirect

Solar Energy Materials & Solar Cells

journal homepage: www.elsevier.com/locate/solmat

Morphology and interdiffusion control to improve adhesion and cohesion properties in inverted polymer solar cells

Stephanie R. Dupont [a], Eszter Voroshazi [b], Dennis Nordlund [c], Reinhold H. Dauskardt [a,*]

[a] Department of Materials Science and Engineering, Stanford University, Stanford, CA 94305-2205, USA
[b] IMEC vzw, Kapeldreef 75, 3000 Leuven, Belgium
[c] Synchrotron Radiation Lightsource, SLAC, Menlo Park, CA, USA

ARTICLE INFO

Article history:
Received 12 June 2014
Received in revised form
29 August 2014
Accepted 9 September 2014
Available online 22 October 2014

Keywords:
Adhesion and delamination
Cohesion
Reliability
Polymer solar cells
Annealing
NEXAFS

ABSTRACT

The role of pre-electrode deposition annealing on the morphology and the fracture properties of polymer solar cells is discussed. We found an increase in adhesion at the weak P3HT:PCBM/PEDOT:PSS interface with annealing temperature, caused by increased interdiffusion between the organic layers. The formation of micrometer sized PCBM crystallites, which occurs with annealing above the crystallization temperature of PCBM, initially weakened the P3HT:PCBM layer itself. Further annealing improved the cohesion, due to a pull-out toughening mechanism of the growing PCBM clusters. Understanding how the morphology, tuned by annealing, affects the adhesive and cohesive properties in these organic films is essential for the mechanical integrity of OPV devices.

1. Introduction

Organic photovoltaic (OPV) devices, typically involving materials that are compatible with flexible plastic substrates, have reached over 10% power conversion efficiency (PCE), one of the critical milestones for market penetration [1–4]. However, organic materials are often mechanically fragile compared to their inorganic counterparts, and devices containing these materials have a higher tendency for adhesive and cohesive failure. For example, the poor adhesion between the poly(3-hexyl)thiophene:[6,6]-phenyl-C61-butyric acid methyl ester (P3HT:PCBM) and poly(3,4-ethylenedioxythiophene) poly(styrene-sulfonate) (PEDOT:PSS), and the low cohesion of the P3HT:PCBM layer can contribute to low processing yield and poor long-term reliability [5,6]. Several methods have been used to increase the fracture properties of OPVs, including polymer:fullerene ratio, molecular weight, polymer layer thickness, chemical treatments and post-electrode deposition annealing [6–10]. The role of pre-electrode deposition annealing has not been studied yet, while it is well known that it strongly affects the bulk heterojunction (BHJ) morphology, phase separation, the carrier mobilities and power conversion efficiency (PCE).

Here, we show how to tune the pre-electrode annealing parameters to control the interdiffusion and morphology of the polymer layers and to optimize the fracture properties. Using Near Edge X-Ray Absorption Fine Structure (NEXAFS) and X-ray Photoelectron Spectroscopy (XPS), an increase of P3HT:PCBM and PEDOT:PSS interdiffusion with annealing temperature was found to be the underlying mechanism for effectively improving the interlayer adhesion, similar to the mechanisms that occur during post-electrode deposition annealing, for all samples that where annealed below the cold crystallization temperature, T_c, of PCBM around 120 °C [11,12].

For annealing above T_c, we found the formation of micrometer large PCBM clusters form, weakening the BHJ layer, even at very short annealing times of 10 min. With further annealing time, the PCBM clusters grew and improved the cohesion of the BHJ, related to a pull-out mechanism of the 100 nm's high PCBM clusters. This behavior was modeled with micromechanical bridging theories. We also found that PCBM cluster formation and extensive phase separation decreased the device PCE due to decreased exciton splitting and hindered charge transport. In conclusion, pre-electrode deposition annealing at temperatures below the T_c of the fullerene can be used to effectively improve the adhesion at the P3HT:PCBM/PEDOT:PSS interface, but annealing above T_c should be avoided to preserve the cohesion and efficiency of the OPV devices.

* Corresponding author. Tel.: +1 650 725 0679; fax: +1 650 725 4034.
E-mail address: dauskardt@stanford.edu (R.H. Dauskardt).

http://dx.doi.org/10.1016/j.solmat.2014.09.013
0927-0248/

2. Experimental section

2.1. Solar cell preparation

Inverted OPV devices with ITO/ZnO/P3HT:PCBM/PEDOT:PSS/Ag architecture were made on 30 mm × 30 mm square glass substrates (Fig. 1). The details of the OPV sample preparation have been reported previously [6,13]. Shortly, ITO coated glass substrates were purchased from Kintec. ZnO was spin coated from a ZnO precursor (zinc acetate dehydrate dissolved in 2-ethoxyethanol, ethonolamine and ethanol). A 250 nm active layer was deposited from a 1:1 wt% mixture of as purchased P3HT (Rieke Materials) and PCBM (Solenne B.V.) dissolved in o-dichloro-benzene (oDCB). Subsequent to deposition, all blends were annealed at 130 °C for 10 min in an inert atmosphere. A 30 nm PEDOT:PSS layer was deposited from a commercially available water-based dispersion (Baytron PVP AI 4083, Clevios), followed by a pre-electrode deposition annealing treatment, as described below. Then, a silver electrode was thermal evaporated (Ag, 100 nm) on top of the annealed samples. Finally, the solar cells were encapsulated by bonding an identical glass substrate on top of the silver electrode using a brittle epoxy, resulting in a square glass sandwich.

2.2. Pre-electrode annealing treatments

Prior to the deposition of the silver electrode, two different annealing treatments were carried out on the hotplate. Set 1 contained samples that were annealed for 10 min at various temperatures: 45 °C, 65 °C, 85 °C, 105 °C and 130 °C. The samples in Set 2 were annealed at a constant temperature of 130 °C for 10 min, 0.5 h, 1 h, 2 h, 3 h and 24 h. In addition each set contained several non-annealed control samples.

2.3. Characterization before debonding

Photovoltaic characteristics of the OPV devices were measured in ambient atmosphere at room temperature with a Keithley 2602A in two-wire configuration under a Lot Oriel 1000 W Xenon arc lamp filtered by OD0.8 Newport neutral density to obtain 100 mW/cm^2 illumination intensity and AM1.5G spectrum. The lamps intensity was calibrated with an ISE Fraunhofer certified Si photodiode. Ultraviolet–visible absorption measurements were performed on all OPV samples using Perkin Elmer Lambda 900 or 950 UV–vis spectrophotometer to record morphology and reorganization changes in the P3HT:PCBM layer prior to adhesion testing.

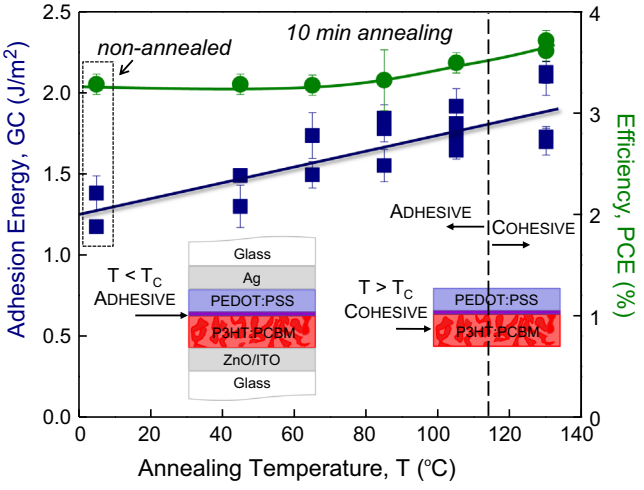

Fig. 1. The measured adhesion energy, G_c (J/m^2) and efficiency, PCE (%) as a function of the 10 min annealing temperature. Insets are illustrations of the OPV device structure with either adhesive or cohesive failure.

2.4. Adhesion specimen and testing

Double cantilever beam (DCB) adhesion specimens of 5 mm wide, 30 mm long and 1.5 mm thick were machined using a high speed wafer saw with a resin blade. To prevent water coolant diffusing into the OPV structure during dicing and damaging the solar cell materials, trenches were cut on each side of square sandwich. Perfectly aligned trenches on the top and bottom glass substrates of the sandwiched structure made it easy to cleave individual DCB specimens prior to testing. The DCB specimens were loaded under displacement control in a thin-film cohesion testing system (Delaminator DTS, Menlo Park, CA) from which a load, P, versus displacement, Δ, curve was recorded. The adhesion energy, G_c (J/m^2), was measured in terms of the critical value of the applied strain energy release rate, G. G_c can be expressed in terms of the critical load, P_c, at which debond growth occurs, the debond length, a, the plain strain elastic modulus, E', of the substrates and the specimen dimensions; width, B and half-thickness, h. The adhesion energy was calculated from Eq. (1) [14]:

$$G_c = \frac{12P_c^2a^2}{B^2E'h^3}\left(1+0.64\frac{h}{a}\right)^2 \quad (1)$$

The debond length was measured directly under an optical microscope and also inferred from measurement of the elastic compliance, dΔ/dP, using the compliance relationship in Eq. (2)

$$a = \left(\frac{d\Delta}{dp}\times\frac{BE'h^3}{8}\right)^{1/3} - 0.64\times h \quad (2)$$

All G_c testing was carried out in laboratory air environment at ~25 °C and ~40% R.H.

2.5. Characterization of the debond path

Following mechanical testing, a survey x-ray photo spectroscopy (XPS, PHI 5000 Versaprobe) scan (0–1000 eV) was made of each of the fractured specimens using monochromatic Al Kα x-ray radiation at 1487 eV in order to characterize the surface chemistry and to help precisely locate the debond path. Detailed high-resolution XPS scans around the S_{2p} core level (155–175 eV) were made for compositional analysis and further identification of the debond path. Optical microscopy was used to locate and determine the nature of the debond path. Atomic force microscopy (AFM) (XE-70, Park Systems) was used to characterize the surface morphology and roughness in non contact mode.

Carbon K-edge NEXAFS spectra [15] were measured on the bending magnet beam line 8-2 at Stanford Synchrotron Radiation Laboratory (SSRL) [16]. The spherical grating monochromator (500 l/mm) was operated with 40 μm by 40 μm slit with a resulting energy resolution of about 0.3 eV. All samples were mounted on an Aluminum sample bar and electrically connected with carbon tape. The spectra shown in the article were acquired in the Total Electron Yield (TEY) mode, measured via the drain current without bias, i0. The incoming flux was normalized by a gold grid with freshly evaporated gold, positioned upstream of the sample chamber, intercepting 10–20% of the beam intensity. The NEXAFS spectra were collected over the range 250–340 eV at 54°, close to the magic angle, where no angular dependence of states with high molecular symmetry (assuming azimuthal averaging) is expected [Stohr PRB angular dependence] for the surface composition extraction. Before normalization, both the i0 and sample current intensity were subtracted by an offset (resulting from amplifiers and a small contribution from the ion pump to the